eIQ Neutron: Redefining Edge-AI Inference with Integrated NPU and Compiler Innovations

Lennart Bamberg* *Member, IEEE*, Filippo Minnella*, Roberto Bosio *Student Member, IEEE*, Fabrizio Ottati, Yuebin Wang, Jongmin Lee, Luciano Lavagno *Senior Member, IEEE*, Adam Fuks

***Abstract*—Neural Processing Units (NPUs) are key to enabling efficient AI inference in resource-constrained edge environments. While peak tera operations per second (TOPS) is often used to gauge performance, it poorly reflects real-world performance and typically rather correlates with higher silicon cost. To address this, architects must focus on maximizing compute utilization, without sacrificing flexibility. This paper presents the eIQ Neutron efficient-NPU—integrated into a commercial flagship MPU—alongside co-designed compiler algorithms. The architecture employs a flexible, data-driven design, while the compiler uses a constrained programming approach to optimize compute and data movement based on workload characteristics. Compared to a leading embedded NPU and compiler stack, our solution achieves an average speedup of 1.8× (4× peak) at equal TOPS and memory resources across standard AI-benchmarks. Even against NPUs with double the compute and memory resources, Neutron delivers up to 3.3× higher performance.**

***Index Terms*—Edge AI, Computer Architecture, Hardware-Software Co-Design, Neural Processing Unit (NPU), Compiler**

I. Introduction

Cloud-based machine learning (ML) inference incurs significant latency and power overhead due to data transfers between user devices and remote servers. It also raises privacy and availability concerns, particularly in mission-, security-, or safety-critical applications. Consequently, there is growing interest in performing efficient ML inference directly on edge devices, both in industry [1], [2] and academia [3], [4].

Edge devices are typically resource-constrained, necessitating domain-specific accelerators such as neural processing units (NPUs), supported by dedicated compiler frameworks [5]–[9]. These NPUs enable compute-intensive workloads within tight power and memory budgets.

Hardware-software (HW/SW) co-design for NPUs has proven effective in reducing model complexity and improving deployability of modern ML models on resource-constrained systems [10]–[12]. State-of-the-art edge-AI models still exhibit high computational complexity in terms of multiply-and-accumulate (MAC) operations. Consequently, NPUs are often evaluated by peak teraoperations per second (TOPS), defined as twice the number of MAC units multiplied by the clock frequency and divided by 10^{12}. However, peak TOPS is a poor proxy for real-world performance, as many MAC units often remain underutilized during inference. Moreover, high TOPS typically implies increased silicon cost and power density, which is problematic for accuracy-critical applications where aggressive approximations (e.g., analog MAC blocks or ultra-low-bitwidth quantization) are unacceptable.

TABLE I
Effective TOPS of two industry-leading edge NPUs on real-world benchmarks.

NPU	Peak TOPS	ResNet50 V1	EfficientNet Lite0
eNPU	4	0.73	0.82
iNPU	11	0.89	0.26

Table I compares the effective TOPS of two industry-leading edge NPUs: an up to $4\,\mathrm{TOPS}$ embedded NPU (eNPU) [7], integratable into any SoC platform, and an $11\,\mathrm{TOPS}$ integrated NPU (iNPU) [9], tied to a custom AI Vision Processor. Effective TOPS, defined as the ratio of executed operations to inference latency, reveals that both NPUs deliver significantly less than their advertised peak (up to $42\times$ lower). Notably, the $11\,\mathrm{TOPS}$ iNPU does not outperform the $4\,\mathrm{TOPS}$ eNPU.

Therefore, peak TOPS should be replaced by metrics that reflect actual compute utilization under realistic memory and bandwidth constraints. Data movement between compute blocks and memory hierarchies (on- and off-chip) imposes significant performance, area, and power penalties.

In-memory compute architectures reduce these penalties, but require sufficient on-chip memory to store entire models—impractical for modern, large-scale ML models or multi-model deployments in mission-, safety-, or security-critical systems where accuracy and redundancy are essential. Consequently, commercial products favor near-memory-compute NPUs with small, tightly coupled memories and integrated data-mover engines. These architectures enable efficient execution of diverse and complex edge-AI workloads that reside in off-chip DDR or flash memory, offering greater flexibility and scalability than in-memory compute solutions [7], [9].

In this work, we introduce a novel near-memory-compute NPU architecture, called *eIQ Neutron*, and a scalable compilation strategy that jointly optimize hardware and software for efficient edge inference, maximizing performance per peak-TOPS and thereby cost-efficiency. While the NPU and software stack are designed for broad applicability—from low-cost MCUs to high-end MPUs—this paper focuses on a $2\,\mathrm{TOPS}$ implementation integrated into a commercial flagship MPU. The resulting hardware–software system achieves best-in-class efficiency—defined as inference latency relative to available compute—across standard computer vision benchmarks.

* Authors contributed equally to this work.

Lennart Bamberg, Filippo Minnella, Fabrizio Ottati, Michael Wang, Jongmin Lee, and Adam Fuks are with NXP Semiconductors. Roberto Bosio and Luciano Lavagno are with Politecnico di Torino, Italy.

Preprint submitted to IEEE Transactions on Computers

The remainder of this paper is organized as follows: Section II summarizes related work; Section III describes the NPU architecture; Section IV details the software stack and compiler; Section V presents experimental results; and Section VI concludes the paper.

II. Related Work

Efficient edge inference is constrained less by peak MAC throughput than by data movement under tight on-chip memory budgets. Moving tensors—especially to and from off-chip memory—can cost orders of magnitude more energy and cycles than arithmetic, making performance gains dependent on minimizing traffic and maximizing on-chip reuse [13]. This observation has shaped most modern accelerator architectures and compiler strategies for the edge.

Within these constraints, HW/SW co-design is essential. Efficient inference requires joint decisions across the stack: from neural network architecture and quantization schemes to compiler-level optimizations such as operator fusion, tiling, scheduling, and strategic tensor placement within limited SRAM. These transformations expose and exploit the underlying hardware's dataflow model and memory hierarchy.

On the architectural side, research has advanced along several axes, including reconfigurable dataflows, sparsity-aware execution, and precision scaling [14]–[17]. In parallel, compiler technology has evolved from heuristic-based approaches [4], [18], [19] toward formal formulations such as constraint programming to capture the complexity of the joint tiling–scheduling–placement design space [20], [21].

However, many prototypes remain limited by immature tooling, narrow operator support, or lack of reproducible deployment on stable silicon. Thus, our study focuses on NPUs that combine hardware maturity with end-to-end toolchains, enabling benchmarking across all standard vision workloads. Representative state-of-the-art (SOTA) solutions illustrate the range of design philosophies:

Micro-NPUs for deeply embedded systems: These accelerators integrate tightly with application processors and microcontrollers and rely on compiler optimizations such as parameter compression and layer fusion to reduce SRAM usage, while recent iterations add structured sparsity and mixed-precision support [7].

High-throughput systolic arrays: These designs employ INT8 systolic arrays with on-chip SRAM as a managed cache for model parameters. Performance degrades when models exceed this budget, requiring segmentation or pipelined execution across multiple devices [8].

Dataflow-centric fabrics: These architectures adopt a distributed-memory fabric. The corresponding compiler partitions DNN graphs across this fabric, explicitly scheduling computation and buffer placement to exploit locality and sustain utilization [9].

Reconfigurable NPUs with sparsity support: Recent proposals integrate sparsity-aware, reconfigurable NPUs within a flagship mobile SoC, combining fine-grained structured sparsity with flexible dataflows for high utilization and energy efficiency [22].

Despite architectural differences, these NPUs converge on one common paradigm: tight coupling between compiler and hardware to orchestrate memory at fine granularity, with fallback to host resources for unsupported operators. This interplay between architecture and compiler-managed memory hierarchies ultimately defines effective edge-AI performance.

III. NPU architecture

In this section, we will outline the architecture of our *eIQ Neutron* NPU. We start with the principles by which the system is designed before we outline the architectural details.

A. Architectural Principles

A sound processor architecture should be guided by first principles. Below, we outline the key principles derived for designing resource-efficient, domain-specific accelerators in aggressively scaled technology nodes (16 nm and below). Adhering to these technology-aware principles enables higher performance at lower cost.

1) Interconnect-Centric Design: In advanced CMOS nodes, gate capacitances shrink with transistor size, whereas metal-wire capacitances increase with scaling as parasitic coupling capacitances grow with wire density. For example, transferring 256 bits over a 1 mm interconnect in 10 nm consumes more energy than hundreds of integer MAC operations [23]. Interconnects dominate placement density, timing closure, and thus all PPA metrics. Architectures must therefore minimize the global and intermediate interconnect bandwidth requirements for full MAC utilization.

2) Memory Locality and Latency Tolerance: Memory scaling outpaces interconnect scaling but lags transistor scaling. Accessing local SRAM with high bandwidth is acceptable (register-level locality is ideal), whereas higher-level memory—especially off-chip DRAM—must be minimized, as resource-efficient systems cannot afford high DDR bandwidth. Architectures should: tolerate latency via deep pipelining on long interconnect paths to achieve high throughput; and minimize global data movement by high data locality achieved at low local memory capacities.

3) Instruction Overhead Reduction: Programmability remains essential for future-proofing in the rapidly evolving artificial intelligence (AI) domain. However, modern edge inference relies on low-cost, low-bitwidth (8–16 bit) integer arithmetic, where a single RISC instruction fetch, decoding, operand fetch, and result write back has magnitudes higher costs than the core MAC operation [24]. Minimizing these instruction and register accesses overhead per operation demands data-driven, systolic architectures, capable of performing large arithmetic sets per programming step.

B. Neutron Core Architecture

Our accelerator employs a dot-product systolic architecture. Traditional high-throughput systolic arrays rely on numerous wide (32-bit) accumulators—introducing significant wire, logic, and register overhead—and suffer from poor utilization on small workloads. Our dot-product structure eliminates these limitations.

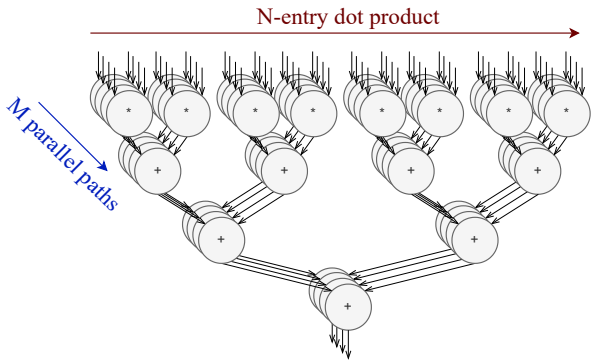

Fig. 1. Core dot-product array.

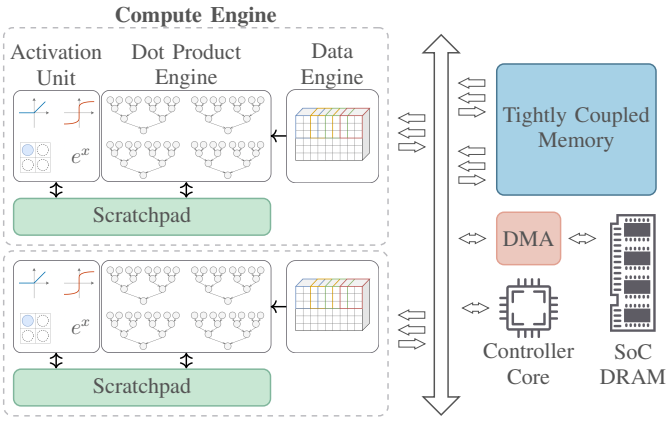

Fig. 2. Proposed Neural NPU subsystem integrated into SoCs.

The core consists of M parallel, pipelined, dot-product units, each completing a dot-product of two vectors of length N per cycle (*cf.* Fig. 1). Thus, it enables $2NM$ operations per cycle. To reduce bandwidth needs, all M units share one operand vector, lowering the required input bandwidth for full utilization from NM (for int8) to N bytes, provided sufficient data parallelism exists. An exception occurs when one operand can remain fully stationary, allowing high utilization even with distinct weights across the parallel units after a short initialization phase.

The compute flow is output-stationary to completely avoid outside memory accesses for wide 32-bit accumulator values. Additionally, A parallel accumulator values per dot-product unit—stored in small local scratchpad memories—enable computing multiple dot-products results concurrently while reusing the second operand. This reduces the bandwidth needs also for the second, non-shared operand by up to a factor $A\times$. Pipelines support 8-bit by 16-bit dot-products using 8-bit multipliers with a two-cycle decomposition, requiring adder trees of 24-bit input and 27-bit output, instead of 16-bit and 19-bit respectively.

Further bandwidth reduction is achieved through a *data engine*: a programmable, word-level pre-fetcher with a multi-dimensional address generation loop fetching in a 2D register file, with support for byte-level scrolling, feeding the dot-product engines. It enables spatial and temporal data reuse, exploiting spatial and temporal locality in AI layers. An optional local scratchpad of size W_C leverages shift invariance in embedding and convolution operations: parameters for the first M pixels/tokens are fetched from external memory, then reused from the cache. If parameters exceed W_C, the layer is partitioned into smaller sub-problems with fewer output features, or the remaining parameters are streamed per set.

Final 32-bit accumulation results can be rescaled to 8 or 16 bits and passed through a dedicated activation engine that applies arbitrary nonlinear functions (e.g., ReLU, Swish, Mish) and supports on-the-fly min/max pooling before writing outputs back to memory. This fusion of operations into a single pipeline further reduces memory bandwidth requirements.

Overall, interconnect and bandwidth demands can be reduced at all ends by tuning M, A, or W_C. Increasing M incurs no local memory, just logic, cost, while A and W_C add minimal scratchpad overhead. Deep pipelining and configurable outstanding transactions on operand and result buses enable high-performance even under high interconnect latency. To minimize programming overhead, the memory-mapped accelerator can execute millions of operations in a single programming step. Next-task programming can overlap with execution to hide latency.

In this work, we configure $N = M = 16$, achieving 0.5 TOPS at 1 GHz per engine with only three 128-bit buses. To further reduce programming overhead and bus utilization at minimal hardware cost, we set $A = 2M$ and $W_C = 8\,\text{kB}$.

C. Neutron Multi-Core System

Fig. 2 illustrates the architecture of the entire NPU subsystem, integrated into several commercial SoCs as an AXI–interconnected accelerator IP. The subsystem comprises a configurable number of the above described compute cores (four in the NPU considered in this work, delivering 2 TOPS), connected via a multilayer bus to a tightly-coupled memory (TCM), a system data mover, and a RISC-V controller core.

Tightly Coupled Memory (TCM): The TCM is a software-managed on-chip memory located near the compute engines, providing high-bandwidth access for neural network data and parameters. It is organized into multiple banks to enable high bandwidth. To maintain high performance at low cost, banks are non-arbitrated; thus, access conflicts must be avoided by the compiler. A virtual-to-physical (V2P) translation table allows dynamic address-to-bank remapping in idle mode.

Controller and Data Movement: The subsystem includes a lightweight RISC-V controller and a direct memory access (DMA) engine for data exchange between the TCM and the rest of the system (e.g., DDR). The DMA supports multi-dimensional strided transfers and TCM-to-TCM data rearrangements, enabling efficient tiling and format transformations (see Section IV-A).

Bandwidth and Control Optimization: To minimize control overhead, avoid Amdahl's law bottlenecks, and reduce memory bandwidth and capacity requirements a multi-layer bus system supports operand sharing across compute engines. The controller can configure operand buses in a sharing mode,

Algorithm 1 Convolution. Nested loops are inlined.

for $h_o \in [0,\ outH),\ w_o \in [0,\ outW),\ c_o \in [0,\ outC)$ **do**
  $a \leftarrow 0$
  for $h_f \in [0,\ filterH),\ w_f \in [0,\ filterW),\ c_i \in [0,\ inpC)$ **do**
    $h_i \leftarrow h_o * S + h_f$ ▷ S: stride.
    $w_i \leftarrow w_o * S + w_f$
    $a \leftarrow a + parameters[c_o,\ h_f,\ w_f,\ c_i] * ifmap[c_i,\ h_i,\ w_i]$
  end for
  $ofmap[h_o,\ w_o,\ c_o] \leftarrow a$
end for

where one operand stream (data or parameters) is broadcast from the TCM to all engines. This requires engines to operate in lockstep on equally sized layer partitions (with optional padding). Programming can be applied globally or per engine, reducing control complexity while maintaining flexibility.

IV. Software stack

The NPU relies on a library of optimized embedded-C kernels implementing layers commonly found in modern ML models, similar in concept to CMSIS-NN or the ATen library [25]. The compiler generates an executable composed of compute jobs, data-transfer jobs, and synchronization barriers for the internal RISC-V controller. Compute jobs invoke the kernel library to program the AI compute cores, while data transfers and synchronization rely on firmware that configures the NPU's DMA engine and monitors execution status.

The compilation flow follows a standard structure: a frontend ingests the neural network model and converts it into an internal intermediate representation (IR); the mid-end lowers and optimizes the graph through tiling, scheduling, and memory allocation; and the backend emits code based on the operator library and firmware, which is compiled into an executable. The host runtime and frontend leverage LiteRT [26] (formerly TensorFlow Lite) for model parsing and fallback execution of unsupported operators, though the mid-end, backend, library, and firmware remain framework-agnostic.

In the remainder of this section, we focus on the novel contribution: how the mid-end leverages constrained programming (CP) based optimization to schedule and allocate resources for the model graph, maximizing utilization under the constraints of the proposed NPU architecture.

A. Format Selection and Tiling

ML models are a good fit for highly-parallel architectures due to the inherent parallelism in the compute tasks. A convolution layer in modern neural networks (NNs) takes two input tensors: an activation tensor, named $ifmap$, of shape ($inpH$, $inpW$, $inpC$); and a weight and bias tensor, named $parameters$, of shape ($outC$, $filterH$, $filterW$, $inpC$). It produces an output tensor, named $ofmap$, of shape ($outH$, $outW$, $outC$). The computation procedure for generating this output tensor is presented in Algorithm 1.

Spatial Tiling: Spatial tiling describes how the computation of a given NN layer is distributed over multiple compute engines. Algorithm 1 reveals that each of the three output dimensions provides parallelism exploitable by spatial tiling.

Algorithm 2 Data distribution among engines in depth parallelism.

parfor $n \in [0,\ N)$ **do**
  $c_{o_{start}} \leftarrow n * \frac{outC}{N}$
  $c_{o_{end}} \leftarrow (n+1) * \frac{outC}{N}$
  $engines[n] \leftarrow ifmap[:,\ :,\ :]$
  $engines[n] \leftarrow parameters[c_{o_{start}} : c_{o_{end}},\ :,\ :,\ :]$
  $engines[n] \rightarrow ofmap[:,\ :,\ c_{o_{start}} : c_{o_{end}}]$
end parfor

Algorithm 3 Data distribution among engines in line parallelism.

parfor $n \in [0,\ N)$ **do**
  $h_{o_{start}} \leftarrow n * \frac{outH}{N}$
  $h_{o_{end}} \leftarrow (n+1) * \frac{outH}{N}$
  $h_{i_{start}} \leftarrow h_{o_{start}} * S$
  $h_{i_{end}} \leftarrow h_{o_{end}} * S + filterH - 1$
  $engines[n] \leftarrow ifmap[h_{i_{start}} : h_{i_{end}},\ :,\ :]$
  $engines[n] \leftarrow parameters[:,\ :,\ :,\ :]$
  $engines[n] \rightarrow ofmap[h_{o_{start}} : h_{o_{end}},\ :,\ :]$
end parfor

When spatially tiling along the channel dimension, $outC$, the same input activations are shared across different filters—increasing efficiency—with each compute engine processing a unique subset of the parameters. We refer to this as *depth parallelism*. Assuming an architecture with N compute engines, as described in Section III, *depth parallelism* is illustrated in Algorithm 2 using NumPy-style [27] tensor slicing syntax.

A key constraint for lockstep execution across compute engines is that each engine must write to a separate memory bank to prevent access conflicts. Hence, $ofmap$ is fragmented in memory along $outC$. This means that $ifmap$, generated by a previous compute job as $ofmap$, is fragmented along $inpC$. Consequently, when broadcasting $ifmap$ to the engines and processing it depth-first, the addressing sequence rotates among the fragments in memory at the word level, as the considered tensor format for compute is *HWC*. This approach eliminates the need for an explicit data rearrangement step to make $ofmap$ contiguous in memory for further processing.

The alternative to depth parallelism is to tile by one of the space coordinates, $outH$ or $outW$. Due to the equivalence of the two variants, we limit our spatial tiling to only consider tiling by $outH$ and refer to it as *line parallelism*. With line-parallel computing, different compute engines work on different output lines but the same output channels. Since parameters and biases in a convolutional operation are independent of the spatial coordinates (enabling translation invariance), *line parallelism* allows the parameters to be shared across the engines to increase efficiency. The locality of the convolution operation requires each compute engine to access different input data windows, which depend on factors like the convolution stride and kernel height. The data distribution for *line parallelism* is shown in Algorithm 3.

To avoid bank access conflicts in line-parallel compute, while achieving lockstep compute, the input windows for each engine must be located in mutually exclusive memory banks. However, when the convolution kernel height exceeds one, these input windows overlap across engines, as illustrated in Algorithm 3. The previous compute, which produced the

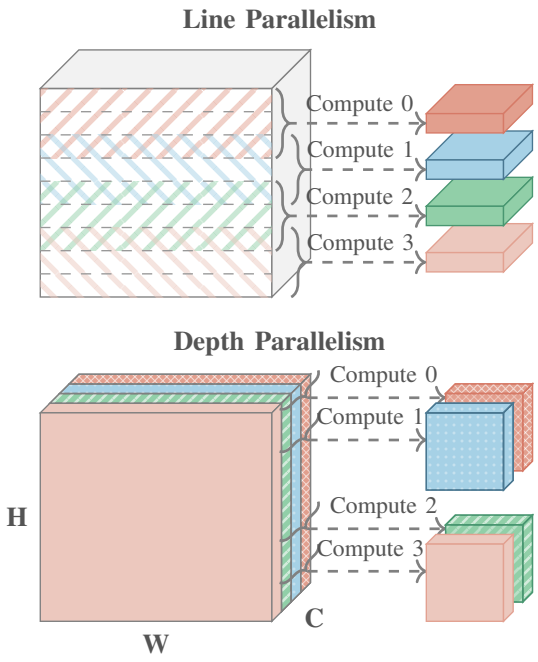

Fig. 3. Data dependencies in depth and line parallelism.

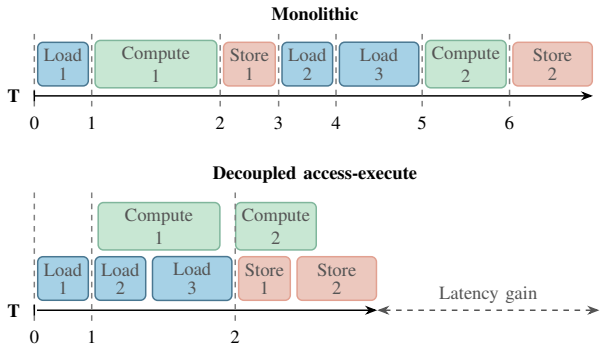

Fig. 4. Comparison between a monolithic and chosen DAE pipeline. In each discrete timestep, multiple datamover jobs can overlap with the computation.

required $ifmap$ as $ofmap$, already wrote the feature map to different banks to avoid access conflicts on result writing. Therefore, before computation can begin, overlapping input regions must be copied between memory banks using TCM-to-TCM transfers. The amount of data to be copied depends on the input-tensor dimensions and convolution properties.

Depthwise convolutions under *depth parallelism* form a special case in which every engine only needs the input channels for the respective output channels it works on. Thus, all engines can work with one of the mutually exclusive subsets of the inputs produced in the previous step without any multi-fragment collection or pre-compute copying.

Fully connected layers and matrix-matrix multiplications are handled as 1×1 convolutions, while element-wise operations like addition and Hadamard layers are interpreted as paired depthwise computations. Scalar operations, such as additions with constants, are similarly treated as 1×1 depthwise operations. Modern Transformer-based neural networks just need considering the embedding dimension as C and and the token dimension as H to obtain the same efficiency gains from the two proposed tiling strategies. Thus, our two-way tiling approach can be applied consistently across all modern NNs.

A visual summary of *line* and *depth parallelisms* is provided in Fig. 3. When the number of tiled lines or channels is not evenly divisible by the number of compute engines N, padding with garbage data is applied to maintain lockstep execution. Furthermore $ifmap$ and $ofmap$ are stored in TCM padded out in C to a multiple of the bus/word-width without increasing compute to make all transactions word aligned. We refer to the memory layouts used by the compute jobs for *line* and *depth parallelisms* as *formats*. Formats are crucial for optimizing compute utilization. The line-parallel format is best suited for shallow layers with few channels but higher resolution. Here, the depth-parallel format often cannot utilize all compute engines. The contrary is true for layers with many channels. Not only because *depth parallelism* allows high compute utilization at low line-counts, but also because it avoids pre-compute TCM copies. The compiler chooses the most suitable format for each layer of the NN by estimating execution latencies and taking into account the overhead of switching formats between consecutive layers, for which extra operators exist in the library.

Temporal Tiling: Once formats are assigned, the next step transforms the tensor-based graph into a tiled representation. Since feature maps may exceed the TCM capacity, layers are divided into smaller tiles, each processed at different times. We refer to this process as temporal tiling. Determining an upper bound for tile size is straightforward: it is enough to ensure that the combined memory footprint of each tile and its required dependencies fits within the TCM. However, such naive bounds are often suboptimal. A more detailed discussion of how temporal tiling is decided is provided in Section IV-C.

B. Scheduling

The scheduling problem involves converting a tile-based graph into a sequence of timed jobs, categorized into two types: data-transfer jobs (pushes, fetches, copies, V2P update) and compute jobs (operator calls). While in literature scheduling often includes determining the tile computation order as well as the tile sizes, this work treats the two aspects separately. Here, scheduling assumes a given sequence of tiles and focuses solely on optimizing memory latency hiding, while ensuring compliance with all platform-specific constraints. A detailed discussion on the selection of an efficient computation order, which is referred to as layer fusion, can be found in Section IV-C.

Time Discretization: The NPU adopts a decoupled access-execute (DAE) architecture, improving resource utilization by memory latency hiding. As illustrated in Fig. 4, this is achieved by allowing compute and datamover jobs to run concurrently. We chose a discretized time (called tick) based time reference for scheduling, implemented in software on the controller core. Without loss of generality, we assume that each timestep can host at most one compute job while allowing an arbitrary number of data-transfer jobs to execute concurrently.

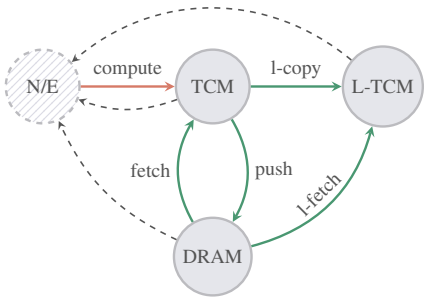

Fig. 5. Tile state diagram. Green arrows indicate transitions performed by the datamover, while the red arrow represents a transition executed by the compute unit.

Under this model, and assuming a valid computation order, computing any tile requires at most three timesteps: one timestep to push the previous results from TCM to off-chip memory, one timestep to fetch the input dependencies and one timestep to perform the actual computation (timesteps for push and fetch may be not used if data can be kept in TCM). This leads to an upper bound on the total number of timesteps needed to compute the entire NN, as well as a clear definition of each tile's lifespan, both of which are key to minimizing the number of variables in the scheduling model.

Variables: In the formulation, tiles are the atomic data blocks, and both operators and data-transfer jobs depend on them. Each tile is modeled according to the state diagram in Fig. 5, which outlines four possible states for each tile:

- *N/E* $\Rightarrow$ outside its lifetime (i.e., not yet generated or no longer needed).
- *DRAM* $\Rightarrow$ stored in off-chip memory.
- *TCM* $\Rightarrow$ stored in TCM.
- *L-TCM* $\Rightarrow$ stored in TCM and expanded to support line-parallel format.

All tiles initially start in the *N/E* state, except for parameters and model inputs which start in *DRAM*. State transitions are depicted by directed arrows; most are managed by the data mover, except for the transition from *N/E* to *TCM*, performed by the compute units. The available transitions are:

- fetch $\Rightarrow$ copy tile from DRAM to TCM.
- push $\Rightarrow$ copy tile from TCM to DRAM.
- compute $\Rightarrow$ compute tile (writes to TCM).
- l-copy $\Rightarrow$ copies a tile within TCM to expand it into the line-parallel format.
- l-fetch $\Rightarrow$ fetches a tile into TCM in line-parallel format directly from DRAM.

While remaining in a state incurs no cost, transitions introduce latency as moving or processing data consumes clock cycles. For completeness, special transitions are represented by dashed arrows, indicating that tile removal occurs without any associated cost, as used memory space can be overwritten. Both transition and states are encoded as boolean variables, and each tile is associated with a set of these variables for every timestep it remains alive.

Constraints: Constraints ensure a valid scheduling behavior, and can be logically classified as follows.

a) Persistency and Transition Constraints: States must persist across consecutive timesteps unless a transition occurs. For a tile j at timestep t, the following constraint ensures that it can only reside in TCM if it was already there at the previous timestep or is being computed or fetched at the current timestep:

$$\begin{aligned}\text{TCM}(j,t-1) + \text{compute}(j,t-1) \\ + \text{fetch}(j,t-1) \geq \text{TCM}(j,t)\end{aligned} \tag{1}$$

Similar constraints are present for the other states and transitions.

b) Dependency Constraints: A tile can only be computed if all its input dependencies are present in TCM. For tile j and its set of dependencies $\text{dep}(j)$, this condition is enforced by:

$$\forall j' \in \text{dep}(j), \quad \text{compute}(j,t) \leq \text{TCM}(j',t) \tag{2}$$

Additionally, symmetric constraints are imposed when the computation requires input tiles to be in a line-parallel format.

c) Bus Constraints: Shared buses between the datamover and the compute unit must not be used concurrently. For a tile j, computed at timestep t, and sharing a bank with an adjacent tile j' of the same tensor, datamover operations on j' must be avoided:

$$\begin{aligned}\text{l-fetch}(j',t) + \text{l-copy}(j',t) \\ + \text{fetch}(j',t) + \text{push}(j',t) = 0\end{aligned} \tag{3}$$

Similar constraints are imposed for tiles that share a bank and are inputs to a computation.

d) Memory Constraints: The total memory consumed by tiles in TCM must not exceed the available TCM. At this stage, each tensor has been already tiled, which means that the bank occupation of each tile is known. For each alive tensor $i \in \mathcal{I}$ at timestep t, let

$$a_{i,j,t} = \begin{cases} 1, & \text{if tile } j \text{ of tensor } i \text{ is active at time } t, \\ 0, & \text{otherwise.} \end{cases}$$

Then, it is possible to define two integer variables that represent the lowest and highest memory bank used per tensor i at timestep t, based on the set of its active tiles:

$$m_{i,t} = \min\{L(j,t) \mid a_{i,j,t} = 1\}. \tag{4}$$

$$M_{i,t} = \max\{H(j,t) \mid a_{i,j,t} = 1\}. \tag{5}$$

where $H(j,t)$ and $L(j,t)$ indicate the highest and lowest bank used by the tile j at timestep t. The inclusion of the timestep in these expressions accounts for memory reuse: under certain conditions, output tiles are allowed to overwrite input tiles, thereby reducing the combined memory footprint. These reuse configurations, specifying which tiles can be overwritten and how many banks are reused, are determined prior to the scheduling phase. Then, the memory occupied by tensor i at time t, independently of where it will be effectively stored in memory, is given by:

$$\text{Mem}_{i,t} = M_{i,t} - m_{i,t} + 1. \tag{6}$$

For each timestep, the total memory occupation over all active tensors must satisfy the constraint

$$\sum_{i\in\mathcal{I}} \text{Mem}_{i,t} = \sum_{i\in\mathcal{I}} M_{i,t} - m_{i,t} + 1 \leq C. \tag{7}$$

where C is the number of TCM banks available.

These constraints collectively define the feasible region for valid scheduling. However, the goal is not just to find any valid schedule but to optimize it for minimal latency. This is achieved by defining an objective function.

Objective Function: The objective function to be minimized represents the total execution latency, computed as the sum of the latencies across all considered timesteps:

$$min \quad \delta N_{DM} + \sum_{t=0}^{\text{T}} max(l_{DM}(t), l_C(t)) \tag{8}$$

where $l_{DM}(t)$ and $l_C(t)$ denote the latencies of the datamover and compute unit at timestep t, respectively, and N_{DM} represents the total number of datamover operations. Since the datamover and compute unit operate in parallel, the latency for a single timestep is determined by the maximum of the two. The additional term δN_{DM} introduces a tuneable penalty to discourage unnecessary datamover operations that are hidden behind computation while still requiring system bus and DDR bandwidth potentially affecting the performance of other components in the the SoC. The CP solver then optimizes the schedule, retaining only the necessary timesteps and eliminating those without any transitions.

Scalability: As each tile is associated with a set of variables for every timestep it remains active, the total number of variables grows linearly with both the number of timesteps and tiles. However, given our time modelization, the total number of timesteps is exactly three times the number of tiles, causing the scheduling problem size to scale quadratically with the number of tiles. As a result, building and solving a single scheduling problem does not scale well with the dimension of the NN. Instead, breaking down the monolithic problem into smaller subproblems significantly improves compilation times. It introduces only a minor performance trade-off, due to a reduced ability to overlap jobs, as the solver no longer has a complete view of the entire scheduling space. Table II shows the impact of this trade-off on a real-case scenario.

C. Optimizations

Temporal tiling is a key aspect of the compilation process. Larger tiles may consume excessive TCM space, leaving insufficient memory for buffering and thus limiting the scheduler's ability to hide memory latency, while overly small tiles may significantly increase compilation time. While most existing approaches emphasize micro-tiling and overlook compilation time as a major factor [20], [28], our approach seeks a balanced compromise between performance and compilation overhead, avoiding excessive trade-offs on either side. Additionally, tile computation order also directly affects latency. In conventional layer-by-layer execution, tiles from different layers cannot be interleaved, requiring all tiles of a layer to be processed consecutively. However, interleaving layer execution, commonly known as layer fusion, can reduce overall off-chip memory usage and thus improve execution latency. As shown in Fig. 6, properly combining layer fusion and tiling can significantly reduce memory requirements in real-world scenarios.

Problem Formulation: The goal is to optimize global memory usage by selecting appropriate tile sizes for each tensor while considering layer fusion. The optimization model used is a simplified variant of the one described in Section IV-B. Unlike the scheduling problem, however, this formulation is not constrained by the actual on-chip memory capacity. Instead, it focuses on minimizing the volume of data that must be offloaded to off-chip memory during scheduling. To this end, the model simplifies the memory hierarchy by considering only a single level, targeting the reduction of total memory usage at each step.

Variables: To determine the optimal tile sizes, dependencies between tensors are ideally analyzed line by line, like in micro-tiling strategies. However, as previously noted, micro-tiling impairs the runtime for complex networks dramatically. To address this, our model simplifies the search space by limiting tile size choices: the largest tile that fits within TCM, and tile sizes reduced by fixed factors. For each feature map i, tiles for each considered size are generated. The selection of the tile size for each data tensor is represented by one boolean variable per size option: $LS_{k,i}$, indicating the selection of the k^{th} biggest tile size for tensor i. Only the tiles of the selected size will allocate on-chip memory. To optimize compiler runtime, in the remainder of this work we consider only two tile-size options per layer.

In this formulation, there is only one memory hierarchy, so for each tile, there are two states:

- *N/E* $\Rightarrow$ the tile is outside its lifetime.
- *TCM* $\Rightarrow$ the tile is stored in TCM.

All tiles initially start in the N/E state, except for parameters and model inputs that are already assumed in TCM. Compute operations move tile states from N/E to TCM.

Because the optimization target is to reduce the on-chip memory overhead, we introduce another integer variable: $MemTh_t$, indicating the memory needed at timestep t of the execution, considering all the tiles in TCM.

Constraints: The constraint expressed in Eq. (7) is modified to take into account the new variable:

$$\sum_{i\in\mathcal{I}} \text{Mem}_{i,t} \leq \text{MemTh}_t. \tag{9}$$

The memory consumption per timestep is not constrained to a fixed value, and the variable $MemTh_t$ is used to track it. Because there is one memory hierarchy, this formulation does not consider the Bus constraints #3. Also, the Persistency and Transition constraints #1 are modified, removing the $fetch$ transition.

Only one tile size is selected for each tensor:

$$\forall i \in \text{tensors}, \quad \sum_{k} \text{LS}_{k,i} = 1 \tag{10}$$

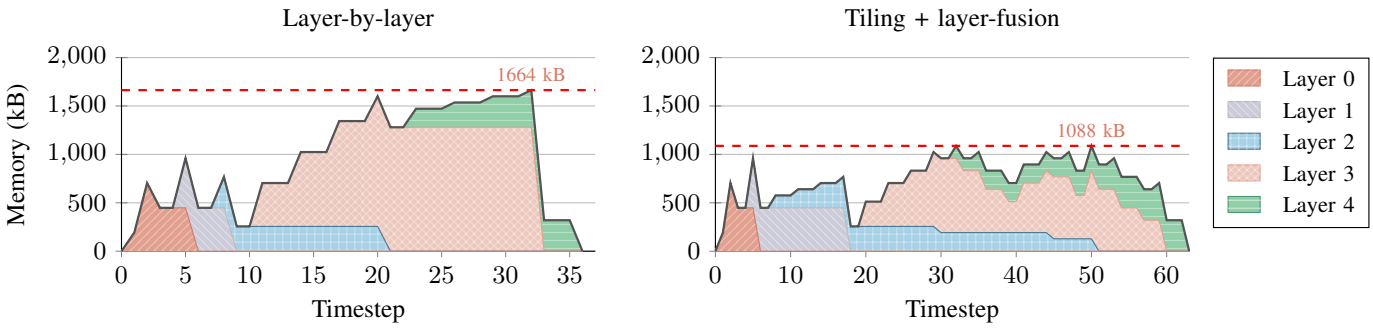

Fig. 6. Memory usage over time during the execution of the first five layers of MobileNetV2, with and without the proposed optimization for layer fusion and tiling. Colored/patterned regions correspond to the memory footprint of individual layers.

TABLE II
IMPACT OF PROBLEM PARTITIONING ON YOLOV8N-DET COMPILATION AND INFERENCE TIMES.

Problem partitioning	Compilation Time (s)	Inference Time (ms)
No partitioning	3480 (0.0%)	23.9 (0.0%)
Only optimizations	1331 (-61.7%)	24.0 (+0.5%)
Only scheduling	1423 (-59.1%)	24.5 (+2.4%)
Both	667 (-80.8%)	24.7 (+3.3%)

Lastly, only tiles related to the selected tile size $LS_{k,i}$ are enabled:

$$\forall j \in tiles, \quad \text{TCM}(j,t) \leq \text{LS}_{k,i} \tag{11}$$

Objective Function: The objective function minimizes the total amount of memory exceeding the on-chip capabilities:

$$min \quad \sum_{t=0}^{\text{T}} MemTh_t - C \tag{12}$$

Scalability: The proposed problem introduces a simplified model that reduces the number of states by half compared to the scheduling formulation and decreases the number of timesteps by a factor of three, as it does not account for additional memory hierarchies. The problem is further decomposed by identifying regions where activation data cannot be held entirely on-chip and restricting layer fusion only to those areas. How this division impacts inference time is evaluated in Table II on a 16-core machine with 32GB of RAM.

D. Memory Allocation

As described in Section III, the virtual mapping of the physical space can be changed through the V2P operation. Given the sequence of timed jobs, the allocation step assigns virtual memory addresses by reserving space for each tile in the virtual view of the TCM. Alongside this, it determines the corresponding physical bank mappings and generates the necessary V2P table updates, ensuring that the compute engine perceives a contiguous view of its data. The constraints defined in the scheduling problem ensure that the TCM space is enough to store all the active tiles in each timestep, guaranteeing that a feasible allocation always exists. However, the allocation step must also account for other architectural choices:

a) Virtual space contiguity: Tiles of the same spatial-tile of a tensor must be stored sequentially in virtual memory. Otherwise, consumers of the tensor may not be able to read it correctly, as the receptive field could span multiple input tiles.

b) Physical space preservation: Tiles must maintain their physical memory banks across time-steps.

c) Reuse optimization: Output tensors must be placed before input tensors in virtual memory, respecting the correct distance, to enable output-input overwriting. This allows consumed data to be overwritten, reducing overall memory usage.

d) Bank exclusivity: Different tensors, used in the same time-step, cannot share the same bank to prevent bus conflicts.

To ensure all these properties are met, the allocation step is formalized as a CP problem, similar to scheduling. Moreover, like the scheduling phase, the allocation problem can be decomposed into smaller subproblems that are solved independently, improving scalability and efficiency.

V. EXPERIMENTAL RESULTS

The performance of the proposed hardware–software system is evaluated on a large set of standard computer vision models for image recognition, object detection, and segmentation. Each model is quantized to INT8 activations and weights and exported to LiteRT v2.18.0. Image-recognition models target the ImageNet dataset [29], while object detection and segmentation models target COCO 2017 [30]. A list of models and their characteristics is provided in Table IV. Real-life (silicon) performance is measured as batch-size-1 end-to-end inference latency on a **production, mass-market micro-processor-unit SoC (MPU)–embedding the proposed 2-TOPS NPU with 1MiB of SRAM and 12GB/s of DDR bandwidth**—employing LiteRT benchmarking tools [39].

To compare our proposed technique with the state-of-the-art, we benchmark all public, general-purpose embedded NPU (eNPU) IPs that allow estimating real-life end-to-end latency on modern AI benchmarks. The results for the eNPU with the best overall peak-performance as well as performance–cost trade-off are used in this paper in two configurations:

a) *eNPU-A*: 2 TOPS, 1 MiB SRAM (64 GB/s), 12 GB/s DRAM.
b) *eNPU-B*: 4 TOPS, 2 MiB SRAM (128 GB/s), 24 GB/s DRAM.

TABLE III
INFERENCE RESULTS ON COMPUTER VISION MODELS. FOR EACH NPU, TOPS, DRAM BANDWIDTH AND SRAM SIZE ARE REPORTED. PERFORMANCE IS ESTIMATED WITH LATENCY AND LTP. THE BEST VALUE PER METRIC IS HIGHLIGHTED.

NPU	**Model**	**Latency [ms]** ↓	**LTP** ↓	—	—	—	—	—	—	—	—	—
Ours (2 TOPS, 12 GB/s, 1 MB)		1.0	**2.1**		0.9	**1.8**		0.8	**1.6**		7.0	**14.0**
eNPU-A (2 TOPS, 12 GB/s, 1 MB)	MobileNet	1.3	2.6	MobileNet	1.5	3.1	MobileNet	1.1	2.1	ResNet	8.5	16.9
eNPU-B (4 TOPS, 24 GB/s, 2 MB)	V1	0.8	3.2	V2	1.0	4.0	V3	**0.7**	2.9	50V1	5.5	22.0
iNPU (11 TOPS)		**0.3**	3.9		**0.3**	3.2		2.0	22.3		**4.5**	49.4
Ours (2 TOPS, 12 GB/s, 1 MB)		1.3	**2.7**		3.6	**7.3**		24.6	49.2		42.5	**85.0**
eNPU-A (2 TOPS, 12 GB/s, 1 MB)	EfficientNet	1.7	3.3	EfficientDet	5.3	10.6	YOLOv8	98.2	196.5	YOLOv8	115.8	231.6
eNPU-B (4 TOPS, 24 GB/s, 2 MB)	Lite0	**1.0**	4.2	Lite0	**3.1**	12.5	N-det.	81.9	327.5	S-det.	91.4	365.8
iNPU (11 TOPS)		3.3	36.5		8.7	95.1		**3.5**	**38.8**		**10.6**	116.9
Ours (2 TOPS, 12 GB/s, 1 MB)		28.7	**57.4**		7.2	**14.4**		2.6	**5.2**		2.7	**5.4**
eNPU-A (2 TOPS, 12 GB/s, 1 MB)	YOLOv8	101.8	203.5	DAMO	8.0	15.9	MobileNet	2.7	5.4	MobileNet	3.2	6.4
eNPU-B (4 TOPS, 24 GB/s, 2 MB)	N-seg.	84.0	335.8	YOLO-NL	**4.0**	16.1	V1 SSD	**1.9**	7.5	V2 SSD	**2.2**	8.8
iNPU (11 TOPS)		**12.9**	141.5		9.0	98.6		4.5	49.2		6.7	73.4

TABLE IV
MODELS USED FOR VALIDATION. DATA RETRIEVED FROM ORIGINAL PAPERS OR OPEN-SOURCE REPOSITORIES [31]–[38]. FOR MOBILENETV3, THE LARGE MINIMALISTIC VARIANT IS USED, AS IT PROVIDES THE HIGHEST ACCURACY UNDER QUANTIZATION. MODEL SIZE IS EXPRESSED AS THE NUMBER OF PARAMETERS.

Classification			**Detection/Segmentation**		
Model	**MACs [G]**	**Size [M]**	—	—	—
MobileNetV1	0.57	4.2	EfficientDet Lite0	1.27	3.9
MobileNetV2	0.30	3.4	YOLOv8N (det.)	4.35	3.2
MobileNetV3 Min	0.21	3.9	YOLOv8S	14.3	11.2
ResNet50V1	2.0	25.6	YOLOv8N (seg.)	6.3	3.4
EfficientNet Lite0	0.41	4.7	MobileNetV1 SSD	1.3	5.1
			MobileNetV2 SSD	0.8	4.3
			DAMO-YOLO Nl	3.0	5.7

Configuration A matches the system resources of our proposed NPU, while configuration B represents a higher-end system with $2\times$ the resources in both DDR bandwidth and TCM capacity, aiming to illustrate that our approach can compete with state-of-the-art designs at half the cost.

In addition to eNPUs, we also compare against all benchmarkable AI-Vision-processor systems with an iNPU below 20 TOPS. For fairness, we include the system with the best performance–cost trade-off on the considered benchmarks in the results presented in this section. This iNPU delivers 11 TOPS and is optimized for computer vision workloads. Exact TCM capacity and DDR bandwidth are not disclosed but are estimated to be in the range of several MiB and 16 GB/s to 24 GB/s, respectively, making its cost in both metrics higher than that of our proposed system integrated into the mass-market MPU.

Performance data for eNPUs and iNPUs is obtained from vendor toolchains and model zoos. Since neither provides area or power estimates, our analysis mainly focuses on performance assessed by means of the batch-size-1 inference latency. Peak TOPS and DDR bandwidth however serve as proxies for area and power, respectively, as MAC units dominate area and DRAM dominates power [23]. In both metrics, our proposed system is better or at least on par with all reference systems.

It is important to note that the iNPU model zoo reports only throughput, which does not directly reflect latency due to the applied inference pipelining. Actual latency exceeds the inverse of throughput, depending on pipeline depth. In the absence of explicit latency data, we approximate latency as the inverse throughput, representing a theoretical lower bound. This may overestimate iNPU performance when latency is the primary concern, but ensures a fair comparison across all reference architectures.

To capture performance efficiency—and thereby power and area—we introduce a second metric in addition to latency: the Latency–TOPS Product (LTP), defined as:

$$\text{LTP} \triangleq \text{latency} \cdot \text{TOPS}, \tag{13}$$

where lower values indicate higher efficiency, meaning less silicon hardware is required to achieve a given performance.

The experimental results are summarized in Table III. Compared to the eNPU with identical resources, our system achieves an average speedup of $1.8\times$ across all benchmarks, with gains up to $4\times$ (YOLOv8N detection). Against the $2\times$ larger eNPU-B, our approach still delivers an average performance uplift of $1.3\times$, peaking at $3.3\times$. Improvements are most pronounced for complex/compute-intensive models such as YOLOv8, demonstrating the superior scalability of our compiler for advanced neural networks.

Even compared to the 11 TOPS iNPU system, our 2 TOPS system achieves an average speedup of $1.25\times$ and up to $2.5\times$ on individual benchmarks—despite having more than $5\times$ fewer TOPS. Across all cases, our design always achieves the best LTP, confirming superior performance-per-cost under strict memory and bandwidth constraints. These findings confirm that intelligent HW/SW co-design, not raw TOPS, determines real-world edge-AI performance.

VI. CONCLUSION AND FUTURE WORK

This work presented a novel, commercial-grade near-memory-compute NPU architecture combined with a constraint-programming-based compiler mid-end. The proposed hardware–software co-design achieves significant performance gains over state-of-the-art solutions while maintaining scalability for modern, high-resolution image segmentation networks—the most computationally demanding edge workloads.

Experimental results demonstrate that our system consistently outperforms industry-leading NPUs across a wide range of benchmarks. Despite operating at only 2 TOPS, it achieves an average speedup of $1.8\times$ over an embedded NPU with identical resources and even surpasses a 11 TOPS AI-Vision-SoC by $1.25\times$ on average. These results highlight a key insight: raw TOPS is a poor predictor of real-world performance. Instead, efficiency at the edge is determined by minimizing data movement and maximizing utilization through intelligent hardware–software co-optimization. Our design delivers superior latency, scalability, and cost-efficiency under strict memory and bandwidth constraints, setting a new benchmark for edge-AI inference.

Although evaluations focused on convolutional models, the proposed framework also supports emerging Gen-AI workloads. Decoder-only Transformer models, which dominate Gen-AI, exhibit highly regular compute patterns (matrix–matrix multiplications), for which we measure tenfold speedups compared to execution on four Cortex-A55 cores at $1.8\times$ the clock frequency. However, fully offloading Gen-AI models to integer NPUs typically degrades accuracy noticeably. Future work will extend the software stack for heterogeneous execution, enabling accuracy-critical but lightweight operations to run in parallel on a floating-point engine with fine-grained synchronization—ensuring true overlap and high utilization of integer-NPU and floating-point compute, rather than the sequential execution seen in current systems.

ACKNOWLEDGMENTS

This result is part of the IPCEI ME/CT and is funded by the European Union Next Generation EU, the German Federal Ministry for Economic Affairs and Energy, the Bavarian Ministry of Economic Affairs, Regional Development and Energy, the Free State of Saxony with the help of tax revenue based on the budget approved by the Saxon State parliament and the Free and Hanseatic City of Hamburg.

REFERENCES

[1] "ExecuTorch: A powerful on-device AI framework," https://github.com/pytorch/executorch, 2024, accessed: March 30, 2025.

[2] R. David, J. Duke, A. Jain, V. Janapa Reddi, N. Jeffries, J. Li, N. Kreeger, I. Nappier, M. Natraj, T. Wang *et al.*, "TensorFlow Lite Micro: Embedded machine learning for TinyML systems," *Proceedings of Machine Learning and Systems*, vol. 3, pp. 800–811, 2021.

[3] J. Lin, W.-M. Chen, Y. Lin, C. Gan, S. Han *et al.*, "MCUnet: Tiny deep learning on IoT devices," *Advances in neural information processing systems*, vol. 33, pp. 11 711–11 722, 2020.

[4] L. Mei, K. Goetschalckx, A. Symons, and M. Verhelst, "DeFiNES: Enabling fast exploration of the depth-first scheduling space for DNN accelerators through analytical modeling," in *2023 IEEE International Symposium on High-Performance Computer Architecture (HPCA)*, 2023, pp. 570–583.

[5] B. Dally, "Hardware for deep learning," in *2023 IEEE Hot Chips 35 Symposium (HCS)*. IEEE Computer Society, 2023, pp. 1–58.

[6] W. J. Dally, Y. Turakhia, and S. Han, "Domain-specific hardware accelerators," *Communications of the ACM*, vol. 63, no. 7, pp. 48–57, 2020. [Online]. Available: https://cacm.acm.org/research/domain-specific-hardware-accelerators/

[7] "Ethos-U85: Advanced NPU with scalable performance and efficiency," 2025, accessed: 2025-04-01. [Online]. Available: https://www.arm.com/products/silicon-ip-cpu/ethos/ethos-u85

[8] "Coral dev board," 2025, accessed: 2025-04-01. [Online]. Available: https://coral.ai/products/dev-board

[9] "Hailo-15 AI vision processor," 2025, accessed: 2025-04-01. [Online]. Available: https://www.hailo.ai/products/ai-vision-processors/hailo-15-ai-vision-processor

[10] L. Deng, G. Li, S. Han, L. Shi, and Y. Xie, "Model compression and hardware acceleration for neural networks: A comprehensive survey," *Proceedings of the IEEE*, vol. 108, no. 4, pp. 485–532, 2020.

[11] B. Jacob, S. Kligys, B. Chen, M. Zhu, M. Tang, A. Howard, H. Adam, and D. Kalenichenko, "Quantization and training of neural networks for efficient integer-arithmetic-only inference," in *Proceedings of the IEEE conference on computer vision and pattern recognition*, 2018, pp. 2704–2713.

[12] A. Kuzmin, M. Van Baalen, Y. Ren, M. Nagel, J. Peters, and T. Blankevoort, "Fp8 quantization: The power of the exponent," *Advances in Neural Information Processing Systems*, vol. 35, pp. 14 651–14 662, 2022.

[13] V. Sze, Y.-H. Chen, T.-J. Yang, and J. S. Emer, "Efficient processing of deep neural networks: A tutorial and survey," *Proceedings of the IEEE*, vol. 105, no. 12, pp. 2295–2329, 2017.

[14] Y.-H. Chen, T. Krishna, J. S. Emer, and V. Sze, "Eyeriss: An energy-efficient reconfigurable accelerator for deep convolutional neural networks," *IEEE Journal of Solid-State Circuits*, vol. 52, no. 1, pp. 127–138, 2017.

[15] D. Kim, J. Ahn, and S. Yoo, "ZeNA: Zero-aware neural network accelerator," *IEEE Design & Test*, vol. 35, no. 1, pp. 39–46, 2018.

[16] J. Sim, J.-S. Park, M. Kim, D. Bae, Y. Choi, and L.-S. Kim, "14.6 A 1.42TOPS/W deep convolutional neural network recognition processor for intelligent IoE systems," in *2016 IEEE International Solid-State Circuits Conference (ISSCC)*, 2016, pp. 264–265.

[17] E. Park, D. Kim, and S. Yoo, "Energy-efficient neural network accelerator based on outlier-aware low-precision computation," in *2018 ACM/IEEE 45th Annual International Symposium on Computer Architecture (ISCA)*, 2018, pp. 688–698.

[18] Y. Xing, S. Liang, L. Sui, X. Jia, J. Qiu, X. Liu, Y. Wang, Y. Shan, and Y. Wang, "DNNVM: End-to-end compiler leveraging heterogeneous optimizations on FPGA-based CNN accelerators," *IEEE Transactions on Computer-Aided Design of Integrated Circuits and Systems*, vol. 39, no. 10, pp. 2668–2681, 2020.

[19] M. Gao, X. Yang, J. Pu, M. Horowitz, and C. Kozyrakis, "TANGRAM: Optimized coarse-grained dataflow for scalable NN accelerators," in *Proceedings of the Twenty-Fourth International Conference on Architectural Support for Programming Languages and Operating Systems*. New York, NY, USA: Association for Computing Machinery, 2019, p. 807–820. [Online]. Available: https://doi.org/10.1145/3297858.3304014

[20] C. Bai, X. Wei, Y. Zhuo, Y. Cai, H. Zheng, B. Yu, and Y. Xie, "Klotski: DNN model orchestration framework for dataflow architecture accelerators," in *2023 IEEE/ACM International Conference on Computer Aided Design (ICCAD)*, 2023, pp. 1–9.

[21] Q. Huang, M. Kang, G. Dinh, T. Norell, A. Kalaiah, J. Demmel, J. Wawrzynek, and Y. S. Shao, "CoSA: Scheduling by constrained optimization for spatial accelerators," in *2021 ACM/IEEE 48th Annual International Symposium on Computer Architecture (ISCA)*, 2021, pp. 554–566.

[22] J.-W. Jang, S. Lee, D. Kim, H. Park, A. S. Ardestani, Y. Choi, C. Kim, Y. Kim, H. Yu, H. Abdel-Aziz, J.-S. Park, H. Lee, D. Lee, M. W. Kim, H. Jung, H. Nam, D. Lim, S. Lee, J.-H. Song, S. Kwon, J. Hassoun, S. Lim, and C. Choi, "Sparsity-aware and re-configurable npu architecture for samsung flagship mobile soc," in *2021 ACM/IEEE 48th Annual International Symposium on Computer Architecture (ISCA)*, 2021, pp. 15–28.

[23] W. J. Dally, "Throughput computing: The quest for efficiency and programmability," Presentation, hosted by UT Austin HPS Group, 2024, accessed: 2025-09-02. [Online]. Available: https://hps.ece.utexas.edu/yale75/dally_slides.pdf

[24] M. Horowitz, "Computing's energy problem (and what we can do about it)," in *2014 IEEE international solid-state circuits conference digest of technical papers (ISSCC)*. IEEE, 2014, pp. 10–14.

[25] P. Contributors, "ATen: A TENsor library," https://github.com/pytorch/pytorch/tree/master/aten, 2025, accessed: 2025-04-01.

[26] G. A. Edge, "LiteRT: High-performance runtime for on-device AI," https://ai.google.dev/edge/litert, 2025, formerly known as TensorFlow Lite.

[27] C. R. Harris, K. J. Millman, S. J. van der Walt, R. Gommers, P. Virtanen, D. Cournapeau, E. Wieser, J. Taylor, S. Berg, N. J. Smith, R. Kern, M. Picus, S. Hoyer, M. H. van Kerkwijk, M. Brett, A. Haldane, J. Fernández del Río, M. Wiebe, P. Peterson, P. Gérard-Marchant, K. Sheppard, T. Reddy, W. Weckesser, H. Abbasi, C. Gohlke, and T. E.

Oliphant, "Array programming with NumPy," *Nature*, vol. 585, no. 7825, pp. 357–362, 9 2020.
[28] A. Symons, L. Mei, S. Colleman, P. Houshmand, S. Karl, and M. Verhelst, "Stream: Design space exploration of layer-fused DNNs on heterogeneous dataflow accelerators," *IEEE Transactions on Computers*, vol. 74, no. 1, pp. 237–249, 2025.
[29] J. Deng, W. Dong, R. Socher, L.-J. Li, K. Li, and L. Fei-Fei, "ImageNet: A large-scale hierarchical image database," in *2009 IEEE Conference on Computer Vision and Pattern Recognition*. IEEE, 2009, pp. 248–255.
[30] T.-Y. Lin, M. Maire, S. J. Belongie, L. D. Bourdev, R. B. Girshick, J. Hays, P. Perona, D. Ramanan, P. Dollár, and C. L. Zitnick, "Microsoft COCO: Common objects in context," *arXiv preprint arXiv:1405.0312*, 2014.
[31] Ultralytics, "YOLOv5 model," https://github.com/ultralytics/yolov5, 2023.
[32] ——, "YOLOv8 model," https://docs.ultralytics.com/models/yolov8, 2023.
[33] A. Howard, M. Sandler, G. Chu, L.-C. Chen, B. Chen, M. Tan, W. Wang, Y. Zhu, R. Pang, V. Vasudevan *et al.*, "Searching for MobileNetV3," *arXiv preprint arXiv:1905.02244*, 2019.
[34] M. Sandler, A. Howard, M. Zhu, A. Zhmoginov, and L.-C. Chen, "MobileNetV2: Inverted residuals and linear bottlenecks," *arXiv preprint arXiv:1801.04381*, 2018.
[35] M. Tan, R. Pang, and Q. V. Le, "EfficientDet: Scalable and efficient object detection," https://github.com/google/automl/blob/master/efficientdet/README.md, 2020.
[36] TensorFlow, "EfficientNet-Lite models," https://github.com/tensorflow/tpu/tree/master/models/official/efficientnet/lite, 2020.
[37] TorchVision, "ResNet-50 model," https://pytorch.org/vision/main/models/generated/torchvision.models.resnet50.html, 2023.
[38] X. Xu, Y. Jiang, W. Chen, Y. Huang, Y. Zhang, and X. Sun, "DAMO-YOLO: A report on real-time object detection design," *arXiv preprint arXiv:2211.15444*, 2022.
[39] "Tensorflow lite benchmark tool," https://github.com/sourcecode369/tensorflow-1/blob/master/tensorflow/lite/tools/benchmark/README.md, 2025, accessed: 2025-04-09.

Biography Section

Lennart Bamberg received the Ph.D. degree with *summa cum laude* in Electrical & Computer Engineering from the University of Bremen, Germany. He is a Chief Processor Architect at NXP Semiconductors, Hamburg, Germany, where he leads the Advanced Computer Architecture Group. His research focuses on domain-specific architectures for machine learning and resource-efficient systems. He has authored numerous publications, holds several patents, and his work has received multiple Best Paper Awards. Dr. Bamberg holds teaching appointments at the University of Bremen and the Technical University of Hamburg.

Filippo Minnella received the Ph.D in Electrical, Electronics and Communications Engineering from Politecnico di Torino in 2023. He worked for STMicroelectronics Automotive group as IC Designer focusing on digital circuits for mixed-signal devices and developing different SoC solutions. He is currently working at NXP Semiconductors Germany as Principal Processor Architect for the proprietary NPU.

Roberto Bosio received the Master's Degree from Politecnico di Torino in 2022. He started his PhD at Politecnico di Torino in the following year. His main interests are High-Level Synthesis and dataflow architectures.

Fabrizio Ottati received his Ph.D. in Electronic Engineering from Politecnico di Torino in 2023. He is currently a Senior Computer Architect at NXP. His research interests include hardware/software codesign of machine learning accelerators and systems.

Yuebin Wang received the B.S. degree in communication engineering from Soochow University, Suzhou, China, in 2016, and the M.S. degree and Ph.D. degree in electrical engineering from Fudan University, Shanghai, China, in 2019 and 2023. Currently, he is a Principle Processor architect with NXP semiconductor in Eindhoven, Netherlands. His research interests include Edge-AI and signal processing.

Jongmin Lee is a Principal Machine Learning Architect at NXP Semiconductors in Austin, TX, USA. Throughout his career at NXP, he has primarily focused on developing MCU-based machine learning solutions and is currently advancing NPU architecture. He earned his Ph.D. in Electrical Engineering from Arizona State University in 2017. He holds a B.S. in Electrical Communications Engineering from Konkuk University and an M.S. from the Korea Advanced Institute of Science and Technology (KAIST). Prior to his doctoral studies, he was a Research Engineer at KAIST Institute, where he contributed to several patents.

Luciano Lavagno (SM'89) received the Ph.D. degree in electrical engineering and computer science from U.C. Berkeley in 1992. He was an Architect with the POLIS HW/SW co-design tool. From 2003 to 2014, he was an Architect with the Cadence C to Silicon high-level synthesis tool. Since 1993, he has been a Professor with the Politecnico di Torino, Italy. He co-authored four books and over 200 scientific papers. His research interests include synthesis of asynchronous circuits, HW/SW codesign and high-level synthesis.

Adam Fuks is a Fellow in Processor Architecture at NXP Semiconductors, based in San Jose, CA, USA. He has over two decades of experience in microcontroller and processor design, specializing in low-power architectures, security, and scalable compute subsystems for edge and embedded systems. At NXP, he drives architectural strategy and innovation across heterogeneous compute platforms and leads initiatives for next-generation AI-enabled processors. Adam holds numerous patents in processor and system architecture and has played a key role in defining industry-leading microcontroller platforms.